RSC Advances

ROYAL SOCIETY OF CHEMISTRY

www.rsc.org/advances

Cite this: DOI: 10.1039/c0xx00000x

COMMUNICATION

One-pot synthesis of 3-D dandelions-like architectures constructed by rutile TiO_2 nanorods grown along [001] axis for high-rate lithium ion batteries

Yu Bai,[a] Naiqing Zhang, *[,a,b] and Kening Sun*[,a,b]

Received (in XXX, XXX) XthXXXXXXXXX 20XX, Accepted Xth XXXXXXXXX 20XX
DOI: 10.1039/b000000x

Novel dandelions-like rutile TiO_2 superstructures are synthesized through a facile one-pot hydrolysis route. The as-prepared structures are composed of inter-aggregated straight nanorods, which are constructed from nanosized rutile TiO_2 (~6 nm) grown along [001] direction. The as-derived TiO_2 shows a high reversible lithium storage capacity of 242 mAh g^{-1} and an excellent rate capability of 116 mAh g^{-1} at 20 *C*.

Introduction

In recent years, lithium ion batteries (LIBs) have attracted considerable attention as a leading candidate for hybrid electric vehicles (HEVs) and electric vehicles (EVs) in view of the gradual depletion of oil resources and global warming.[1] However, the traditional carbonaceous anodes of the commercial LIBs can not satisfactorily meet the safety requirments in the future applications of HEVs and EVs. To solve this problem, many efforts have been focused on exploiting alternative anode materials. TiO_2 has been regarded as a promising anode material for high power LIBs[2,3] owing to its inherent advantages. Compared to graphite, the TiO_2 shows higher lithium insertion potential (1–3 V *vs*. Li/Li^+), which could prevent the formation of dendritic lithium during the charge-discharge process. Moreover, the TiO_2 features negligible volume change (< 1%) during the charge-discharge process, which could ensure an excellent reversibility and structure stability in a long-term cycle. TiO_2 polymorphs include rutile, anatase, brookite, and TiO_2-B. Up to now, the investigations are mainly focused on anatase[4] and TiO_2-B[5]. Although rutile (P42/mnm) is the most common and thermodynamically stable form of TiO_2, there are few reports on Li^+ insertion properties of rutile TiO_2. The primary reason is that the bulk rutile can only accommodate a negligible amount of Li^+ (<0.1 Li^+ per TiO_2 unit) due to kinetic restrictions.[3a,6]

To overcome this issue, rutile TiO_2 has been prepared as nanosized or mesoporous particles to increase the electrode/electrolyte contact area and shorten the Li^+ diffusion length in the solid phase, facilitating for Li^+ insertion/extraction.[7] Recently, the reversible capacity of rutile TiO_2 was greatly increased to 200 mAh g^{-1} (~0.6 Li/Ti),[7a,7d] which is even superior to that of most nanosized anatase (168 mAh g^{-1}, ~0.5 Li/Ti). However, the capacities of the as-reported nanosized rutile TiO_2 are still lower than its theoretical capacity value (~0.85 Li/Ti),[8] since the diffusion of Li^+ in rutile is highly anisotropic in the tetragonal rutile (P42/mnm) special arrangement. Experimental results and simulations have revealed that the Li^+ diffusion coefficient along the *c*-direction is approximately 10^{-6} cm^2 s^{-1}, which is much higher than that in the *ab*-plane (10^{-15} cm^2 s^{-1}).[3a,6a] Therefore, the migration of Li^+ in rutile TiO_2 is nearly confined along the *c*-axis channels. In this context, constructing superstructures composed of nanosized rutile TiO_2 grown along *c*-axis which makes all the Li^+ diffusion channels available from the surface is of great significance for enhancing its electrochemical performance.

Herein, we report the synthesis of "dandelion" rutile TiO_2 through a facile one-pot hydrolysis route by employing titanium tetrachloride ($TiCl_4$) as the titanium source and 1-hexadecyl-3-methyl imidazolium bromine (C16mimBr) as the structure-directing agent. The TiO_2 nanostructure is composed of inter-aggregated straight nanorods grown along *c*-axis, which facilitates the transport of lithium ions and electrons. The as-prepared rutile TiO_2 exhibits a high reversible capacity of 242 mAh g^{-1} (~0.72 Li/Ti) and a high rate capacity of 116 mAh g^{-1} at 20 *C* with an excellent cycle life.

Experimental

Synthesis of rutile TiO_2

In a typical synthesis process of hierarchical nanostructured rutile TiO_2, we employ $TiCl_4$ as precursor, and C16mimBr as solvent and structure-directing agent. The chemical structure of C16mimBr is shown schematically below.

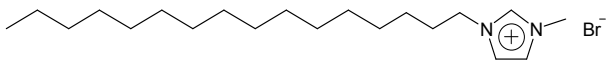

1.1 mL of $TiCl_4$ was dropwise added into 5.4 mL of distilled water mixed with 3.23 g of C16mimBr in an ice bath, stiring strongly to form a clear solution. Thereafter, in order to achieve highly ordered superstructures, the solution was heated to 100 °C for another 12 h under stong stiring to control the hydrolysis of $TiCl_4$ in the solution. The obtained dispersion was diluted with 20 mL of anhydrous ethanol, then gathering the product by centrifugation. The residual of C16mimBr in the product was

removed by extracting the sample with acetonitrile at 100 °C. we carry out Fourier transform infrared (FTIR) measurement to see if there is some residual C16mimBr in our sample. As shown in Fig. S1 and Fig S2, the imidazolium *v* (C–H) stretching region (3200–3000 cm^{-1}) of the C16mimBr disappears, indicating that the C16mimBr is completely removed.

Physics Characterisation

The resulting samples were characterized by means of X-ray diffraction (XRD, Rigaku D/max-γB) with monochromated Cu Kα radiation at a scanning rate of 2 ° min^{-1} in the range of 10–70 °. The morphology of the synthesized materials was examined using a scanning electron microscopy (SEM, Hitachi S4800) and the microstructure of the powders was observed by a high resolution transmission electron microscopy (HRTEM, Hitachi 7650) operating at 300 kV. Before TEM and HRTEM characterizations, the TiO_2 sample was dried and then dispersed thoroughly in ethanol by untrasonic method. The as-obtained suspension was droped onto a 400-mesh carbon-coated copper grid and left in air to dry. The surface area for powdered sample was measured by the Brunauer-Emmett-Teller (BET) method using ASAP2020.

Cell fabrication and electrochemical characterizations

The anode film studied here was prepared by mixing the TiO_2 powder, carbon black and polyvinylidene fluoride with a weight ratio of 8:1:1 in N-methyl pyrrolidinone. The slurry was coated onto an aluminum foil by the "doctor blade" technique and dried under vacuum at 120 °C over night. The electrode was roll-pressed under an appropriate pressure to enhance the adhesion. The anodes typically had an active material loading of 2.4–3.2 mg and their loading differences for the same electrochemical test were less than 0.15 mg. The compact density and thickness of anodes were 0.75 g cm^{-3} and 20–30 μm, respectively. Coin type (CR2025) test cells were assembled in an Mbraun argon-filled glove box (O_2 < 1 ppm and H_2O < 1 ppm) using two porous polypropylene films as a separator, 1 M $LiPF_6$ in ethylene carbonate, dimethyl carbonate and ethylmethyl carbonate (EC/DMC/EMC, 1:1:1 vol) as electrolyte, and Li foil as the counter and reference electrodes. Constant current charge/discharge was performed at various rates within a voltage window of 1–2.5 V (vs. Li/Li^+). CV measurements were carried out on an electrochemical workstation (CHI, 650B) at a series of sweep rates. Electrical impedance spectroscopy (EIS) experiments were carried out on a Parstat 2273 advanced electrochemical system in the frequency range mainly from 1 MHz to 50 mHz with an amplitude of 10 mV. Before EIS measurements all samples were charged to the same voltage of 1 V.

Results and discussion

The detailed synthesis procedure of rutile TiO_2 is described in Experimental Section. The crystal phase of the as-derived TiO_2 was determined by the X-ray diffraction (XRD) characterization. As shown in Fig.1a, all diffraction peaks can be indexed to TiO_2 crystal with the standard tetragonal rutile pattern (JCPDS. No. 65-0191) and no secondary peak is observed over the entire pattern. Meanwhile, the average crystal size is calculated to be 6.2 nm from the most intense diffraction peak (110) through the Debye-Scherer equation, indicating that the product is composed of pure rutile TiO_2 nanocrystals.

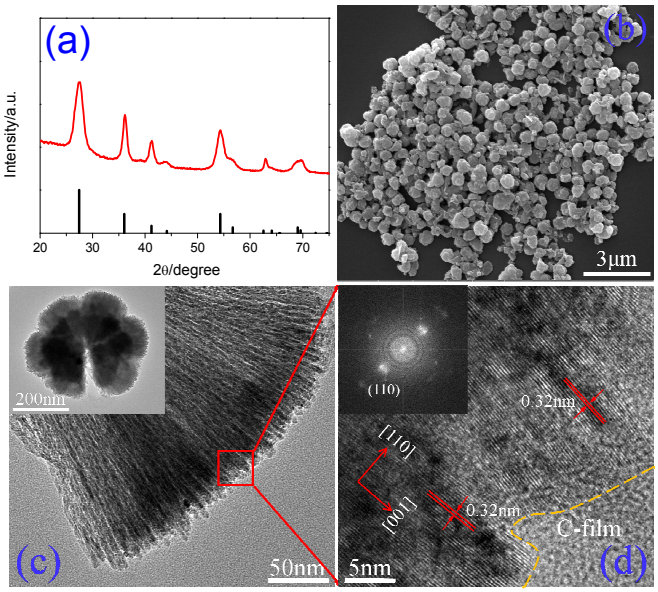

Figure 1. (a) XRD of standard rutile TiO_2 (JCPDS. No. 65-0191) and the as-derived TiO_2. (b) Representative SEM image of rutile TiO_2. (c) TEM images of dandelion-like rutile TiO_2 (the inset shows the TEM image of a TiO_2 particle). (d) HRTEM image of rutile TiO_2(the inset shows the corresponding FFT pattern of the same region).

The panoramic scanning electron microscopy (SEM) image in Fig. 1b shows the existence of uniformly distributed spherical-shaped particles with an average size of 400 nm. The discrepancy of the sizes calculated from XRD and observed in SEM measurements suggests that the as-prepared TiO_2 particles are consist of nanosized subunits.

We further carried out transmission electron microscopy (TEM) measurements to elucidate the intrinsic micro/nano structure of the rutile TiO_2 particles. The TEM image (the inset of Fig. 1c) reveals that the rutile TiO_2 particle features a dandelions-like nanostructure comprised with numerous well-defined and straight nanorods. As shown by the magnified TEM image (Fig. 1c), the nanorods with a diameter of around 6 nm are oriented radially from the central region toward edges of the particle. In addition, the result of the nitrogen adsorption-desorption experiment (Fig. S3 in ESI†) indicates that there exists a large BET specific surface area of 114 $m^2 g^{-1}$ for the dandelions-like TiO_2. Fig.1d shows the high-resolution transmission electron microscopy (HRTEM) image and the corresponding fast Fourier-transform (FFT) pattern of the selected region as marked in Fig. 1c. The crystalline region with clear lattice fringes has an inter-planar spacing of 0.32 nm, which is consistent with the (110) atomic planes of the rutile structure. It indicates that rutile nanorods are single crystalline along the [001] axis. The diffusion ring in the inset of Fig. 1d stems from the amorphous carbon substrate. When we remove the C16mimBr in the synthesis procedure, the nanocrystalline anatase TiO_2 with an average nanoparticles size of ~4 nm is obtained (Fig. S4 and Fig. S5 in ESI†). Therefore, the C16mimBr plays a critical role in controlling the crystal structure and the morphology of TiO_2. As

reported by Chang,[9] the hydrogen atoms in C2 position of imidazole rings have strong hydrogen-bonding interaction with oxygen atoms of the rutile surface. The $[C16mim]^+$ cations can effectively anchor onto the (110) facets of TiO_6 octahedra instead of H^+, forming [C16mim]–O–Ti hydrogen-bonding groups as illustrated in Fig. 2a. The mutual π-π stacking interactions between aromatic rings would induce the formation of linear nuclei *via* edge-sharing TiO_6 octahedra. Meanwhile, the hydrophobic interaction between long alkyl chains can synergetically extend the π-π stacking effect and thus increase the long-range oriented-growth of rutile TiO_2.[10] Therefore, the rutile nanorods grown along [001] axis with a diameter of about 6 nm can be constructed. The rutile nanorods were further assembled into dandelions-like nanoarchitecture, owing to the hydrophobic interactions between the adjacent hydrocarbon chains enwrapped on the surface of the nanorods.

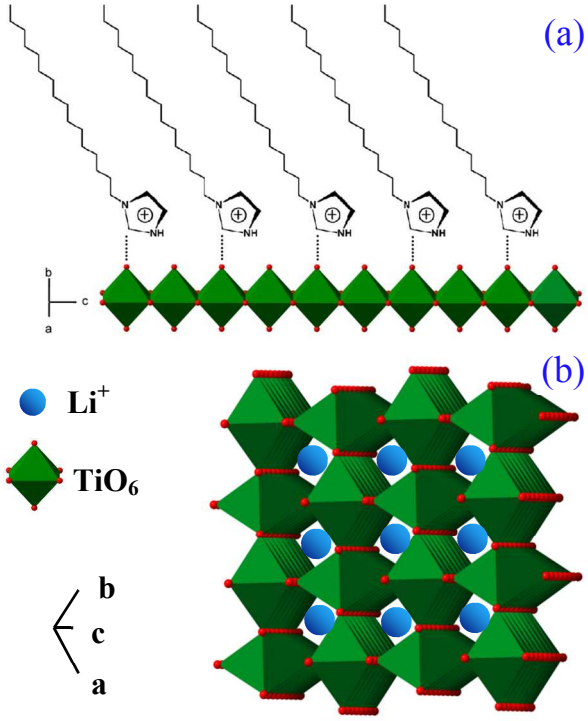

Fig.2 (a) Schematic illustration of a projected view of the nucleation pathways by $[C16mim]^+$ ions anchored onto rutile (110) plane. **(b)** The schematic model of rutile TiO_2 with insertion of Li^+ ions between TiO_6 octahedral voids.

To evaluate the electrochemical characterizations of the as-prepared dandelions-like rutile TiO_2, we first measured its cyclic voltammogram (CV) between 1 and 3V as shown in Fig. 3a. At the first discharge, there are three well-resolved cathodic peaks centered at 1.1, 1.4, and 2.1 V, which disappear in the following cycles. The peaks at 1.1 and 1.4 V can be ascribed to the phase transformation from TiO_2 to Li_xTiO_2, and the peak at 2.1 V is assigned to the irreversible adsorption of lithium ions.[7a] In the subsequent cycles, a pair of broad cathodic/anodic peaks centred at around 1.76 and 1.83 V are associated with lithium insertion/extraction in the Li_xTiO_2. Moreover, the difference between the second cycle and the subsequent cycles is negligible, revealing that the dandelions-like rutile TiO_2 displays a good reversible capacity.

The lithium insertion/extraction properties could be further corroborated by the charge/discharge measurement at a current density of 68 mA g^{-1} (rate = 0.2 *C*) as shown in Fig. 3b. In the first cycle, we observe an irreversible capacity with a discharge capacity of 337 mAh g^{-1} and a charge capacity of 269 mAh g^{-1}. This irreversible capacity is comparable with the values reported by other groups and is normally attributed to the formation of intermediate phase Li_xTiO_2 and the irreversible surface adsorption of lithium ions.[7] During subsequent cycles, the profiles feature almost monotonic voltage evolution without a constant potential region, reflecting the typical behavior of Li^+ insertion/extraction in the Li_xTiO_2. The second charge/discharge curves indicate that about 0.72 Li per mol TiO_2 can be reversibly inserted/extracted, and the corresponding capacity of 242 mAh g^{-1} is much higher than that reported previously.[6,7] In addition, between the second and subsequent cycles, no obvious difference can be observed from the charge/discharge capacities, in agreement with our aforementioned CV results. This behavior could be explained by the fact that rutile TiO_2 nanorods have freely accessible parallel channels along the [001] direction as illustrated in Fig. 2b, in which lithium ions can be accommodated without causing any remarkable distortion of the prepared superstructure.

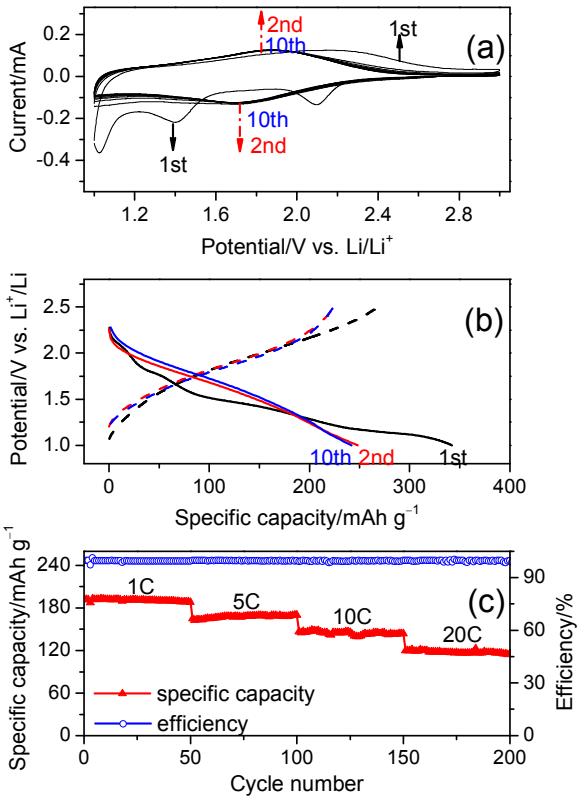

Fig. 3 (a) Cyclic voltammograms of rutile TiO_2 electrode at a scan rate of 0.2 mV s^{-1} for the first 10 cycles. Potentials are measured relative to a Li/Li^+ reference electrode (Potential range: 1 V–3 V). (b) Voltage profiles of initial charge discharge cycles of Li/TiO_2 between 1 V and 2.5 V at a rate of 0.2 *C* (=68 mA g^{-1}). (c) Discharge capacity and coulombic efficiency versus cycle number under different current rates (1 *C*–20 *C*).

The rate capability of the as-derived rutile TiO_2 was further evaluated with charge/discharge rates stepwise increasing from 1

to 20 *C*. For each stage, the cell was cycled for 50 times. As shown in Fig. 3c, the discharge capacities at 1 *C*, 5 *C*, 10 *C* and 20 *C* are around 188, 170, 144 and 116 mAh g^{-1}, respectively. The rate performance of our TiO_2 is superior to that of rutile-TiO_2-based nanomaterials under similar test conditions in previous reports.[6,7] We ascribe the enhanced rate capability to the following reasons: i) for the nanosized TiO_2, the pseudocapacitance contributes obviously to the electrochemical lithium storage and could significantly accelerate the charge/discharge kinetics of the material;[11] ii) the well-connected nanorod-crystals provide a continuous pathway for the diffusion of lithium ions and electrons in the titania scaffold; iii) the special structure exposes plenty of vertical cross-section of *c*-axis as illustrated in Fig. 2b, thus enlarging the effective contact area for the transport of Li^+.

In addition, the rutile TiO_2 exhibits excellent cyclability, retaining over 97% of its initial capacity after 50 cycles at all rates. Impedance analysis was further carried out after various numbers of cycles (including 1st, 50th, 100th, 200th). As shown in Fig. 4, the EIS spectra consists of a semicircle and a slope, referring to the charge transfer reaction and the diffusion of Li^+ in the bulk electrode, respectively.[12] During our experiment, the values of charge-transfer resistence (R_{ct}) are all lower than 70 Ω, implying negligible structure change of dandelions-like rutile TiO_2 during cycling process. The SEM and TEM measurements for the TiO_2 anode after 200 cycles (Fig. S6) further confirms little structure change of the TiO_2 nanorods after the cycling process.

Furthermore, the coulombic efficiencies approach 100% even at higher identical charge and discharge rates (right ordinate of Fig. 3c). The good electrochemcal performance in combination with a facile preparation procedure makes the described dandelions-like rutile TiO_2 a promising electrode material for lithium ion batteries.

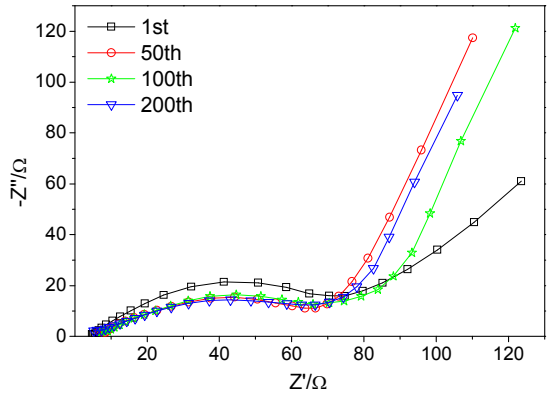

Fig. 4 EIS data at different stages.

To summarize, we have synthesized a dandelions-like rutile TiO_2 superstructure through a facile one-pot hydrolysis route by employing titanium tetrachloride as the titanium source and C16mimBr as the structure-directing agent. The dandelion-like particles with the average size of 400 nm are comprised of inter-aggregated straight rods, which constructed from nanosized rutile TiO_2 (~6 nm) grown along [001]. The cell assembled with dandelions-like rutile TiO_2 shows high reversible lithium storage capacity and excellent rate capability. The strategy of constructing dandelions-like superstructures demonstrated in this work may be potentially extendable to other lithium insertion host materials for future improvement of their specific capacities and rate performance.

This project is supported by the National Natural Science Foundation of China (No. 51203036), the China Postdoctoral Science Special Foundation (2013T60380), the China Postdoctoral Science Foundation (2012M520748), and the "Young Talent Program" of Harbin Institute of Technology. We are grateful to Lanzhou Greenchem ILS, LICP. CAS. China for supplying C16mimBr. The authors also thank Dr. Yunfeng Qiu from Academy of Fundamental and Interdisciplinary Sciences, Harbin Institute of Technology, for his constructive suggestions.

Notes and references

[a] *Academy of Fundamental and Interdisciplinary Sciences, Harbin Institute of Technology, Harbin, 150001, China. Fax: +86 451 86412153; Tel: +86 451 86412153; E-mail: keningsunhit@126.com, znqmww@126.com*

[b] *State Key Laboratory of Urban Water Resource and Environment, Harbin Institute of Technology, Harbin, 150090, PR China.*

† Electronic Supplementary Information (ESI) available: Additional data analysis. See DOI:

1 (a) M. Armand and J. M. Tarascon, *Nature*, 2008, **451**, 652; (b) P. G. Bruce, B. Scrosati and J. M. Tarascon, *Angew. Chem. Int. Ed.*, 2008, **47**, 2930.

2 G. Nuspl, K. Yoshizawa, T. Yamabe, *J. Mater. Chem.*, 1997, **7**, 2529.

3 (a) D. Deng, M. G. Kim, J. Y. Lee, J. Cho, *Energy Environ. Sci.*, 2009, **2**, 818; (b) T. Djenizian, I. Hanzu, P. Knauth, *J. Mater. Chem.*, 2011, **21**, 9925; (c) G. Jeong, Y.-U. Kim, H. Kim, Y.-J. Kim, H.-J. Sohn, *Energy Environ. Sci.*, 2011, **4**, 1986. (d) A. I. Hochbaum, P. Yang, *Chem. Rev.*, 2010, **110**, 527; (e) Z. Yang, D. Choi, S. Kerisit, K. M. Rosso, D. Wang, J. Zhang, G. Graff, J. Liu, *J. Power Sources*, 2009, **192** 588; (f) P. G. Bruce, B. Scrosati, J. M. Tarascon, *Angew. Chem. Int. Ed.*, 2008, **47**, 2930.

4 (a) M. Wagemaker, A. P. M. Kentgens, F. M. Mulder, *Nature*, 2002, **418**, 397; (b) K. X. Wang, M. D. Wei, M. A. Morris, H. S. Zhou, J. D. Holmes, *Adv. Mater.*, 2007, **19**, 3016; (c) S-M. Paek, J-H. Kang, H. Jung, S-J. Hwanga, J-H. Choy, *Chem. Commun.*, 2009, **48**, 7536; (d) S. Liu, G. L. Pan, N. F. Yan and X. P. Gao, *Energy Environ. Sci.*, 2010, **3**, 1732; (e) J. S. Chen, Y. L. Tan, C. M. Li, Y. L. Cheah, D. Y. Luan, S. Madhavi, F. Y. C. Boey, L. A. Archer, X. W. Lou, *J. Am. Chem. Soc.*, 2010, **132**, 6124; (f) K. Saravanan, K. Ananthanarayanan, P. Balaya, *Energy Environ. Sci.*, 2010, **3**, 939; (g) C. H. Sun, X. H. Yang, J. S. Chen, Z. Li, X. W. Lou, C. Li, S. C. Smith, G. Q. Lu, H. G. Yang, *Chem. Commun.*, 2010, **46**, 6129; (h) J. S. Chen, D. Luan, C. M. Li, F. Y. C. Boey, S. Qiao, X. W. Lou, *Chem. Commun.*, 2010, **46**, 8252; (i) S. Ding, J. S. Chen, D. Luan, F.Y. C. Boey, S. Madhavi, X. W. Lou, *Chem. Commun.*, DOI: 10.1039/c1cc10687b.

5 (a) A. R. Armstrong, G. Armstrong, J. Canales, P. G. Bruce, *Angew.Chem. Int. Ed.*, 2004, **43**, 2286; (b) G. Armstrong, A. R. Armstrong, J. Canales, P. G. Bruce, *Chem. Commun.*, 2005, **44**, 2454; (c) J. Li, W. Wan, H. Zhou, J. Li, D. Xu, *Chem. Commun.*, 2011, **47**, 3439; (d) A. R. Armstrong, C. Arrouvel, V. Gentili, S. C. Parker, M. S. Islam, P. G. Bruce, *Chem. Mater.*, 2010, **22**, 6426; (e) H. Kaper, S. Sallard, I. Djerdj, M. Antonietti, B. M. Smarsly, *Chem. Mater.*, 2010, **22**, 3502.

6 (a) W. J. Macklin, R. J. Neat, *Solid State Ionics*, 2003, **157**, 35; (b) Y-S. Hu, L. Kienle, Y.-G. Guo and J. Maier, *Adv. Mater.*, 2006, **18**, 1421.

7 (a) E. Baudrin, S. Cassaignon, M. Koesch, J. P. Jolivet, L. Dupont, J. M. Tarascon, *Electrochem. Commun.*, 2007, **9**, 337; (b) C. H. Jiang,

I. Honma, T. Kudo, H. S. Zhou, *Electrochem. Solid-State Lett.*, 2007, **10**, A127; (c) P. Kubiak, M. Pfanzelt, J. Geserick, U. Homannc, N. Husing, U. Kaiserc, M. Wohlfahrt-Mehrensa, *J. Power Sources*, 2009, **194**, 1099; (d) M. Pfanzelt, P. Kubiak, M. Wohlfahrt-Mehrens, *Electrochem. Solid-State Lett.*, 2010, **13**, A91; (e) Y. Jin, Y. Liu, Y. Wang, X. Li, S. Hu, W. Li, *International Journal of Minerals, Metallurgy and Materials*, 2012, **19**, 1058;

8 M. Wagemaker, W. J. H. Borghols, U. Lafont, E. M. Kelder, F. M. Mulder, *Chem. Mater.*, 2008, **20**, 2949.

9 J-G, Chang, J. Wang, M. C. Lin, *J. Phys. Chem. A*, 2007, **111**, 6746.

10 Y. Zhou, J. H. Schattka, M. Antonietti, *Nano Lett.,* 2004, **4**, 477.

11 (a) T. Brezesinski, J. Wang, J. Polleux, B. Dunn, S. H. Tolbert, *J. Am. Chem. Soc.*, 2010, **131**, 1802. (b) J. Wang, J. Polleux, J. Lim, B. Dunn, *J. Phys. Chem. C*, 2007, **111**, 14925.

12 Liu, H.; Feng, Y.; Wang, K.; Xie, J. *J. Phys. Chem. Solids*, 2008, **69** 2037.